


Article

Seismological Observations of Ocean Swells Induced by Typhoon Megi Using Dispersive Microseisms Recorded in Coastal Areas

Jianmin Lin ^{1,2,*} , Sunke Fang ¹ , Xiaofeng Li ³ , Renhao Wu ¹  and Hong Zheng ^{1,*}

¹ Marine Acoustics and Remote Sensing Laboratory, Zhejiang Ocean University, Zhoushan 316021, China; fangsunke@outlook.com (S.F.); mikewu@zjou.edu.cn (R.W.)

² State Key Laboratory of Acoustics, Institute of Acoustics, Chinese Academy of Sciences, Beijing 100190, China

³ Global Science and Technology, National Oceanic and Atmospheric Administration (NOAA)-National Environmental Satellite, Data, and Information Service (NESDIS), College Park, MD 20740, USA; xiaofeng.li@noaa.gov

* Correspondence: jmlin007@zjou.edu.cn (J.L.); seahzheng@msn.com (H.Z.); Tel.: +86-580-218-3617 (J.L.); +86-580-255-0753 (H.Z.)

Received: 14 August 2018; Accepted: 6 September 2018; Published: 8 September 2018



Abstract: Typhoons in the western Pacific Ocean can generate extensive ocean swells, some of which propagate toward Taiwan, Luzon, and the Ryukyu Islands, impacting the coasts and generating double-frequency (DF) microseisms. The dispersion characteristics of DF microseisms relevant to the propagation of ocean swells were analyzed using the fractional Fourier transform (FrFT) to obtain the propagation distance and track the origins of typhoon-induced swells through seismic observations. For the super typhoon Megi in 2010, the origin of the induced ocean swells was tracked and localized accurately using seismic records from stations in eastern Taiwan. The localized source regions and calculated wave periods of the ocean swells are in good agreement with values predicted by ERA5 reanalysis from the European Centre for Medium-Range Weather Forecasts (ECMWF). However, localized deviations may depend on the effective detection of dispersive DF microseisms, which is tied to both coastline geometry and the geographic locations of seismic stations. This work demonstrates the effectiveness of seismological methods in observing typhoon-induced swells. The dispersion characteristics of DF microseisms recorded by coastal stations could be used as a proxy measure to track and monitor typhoon-induced swells across oceans.

Keywords: typhoon; ocean swell; microseism; seismic station

1. Introduction

Swells induced by a typhoon can be devastating and commonly cause major damage to ships and coastal infrastructure, as they can propagate over long distances with their energy only weakly attenuated [1,2]. In addition to strong societal and environmental consequences, swells can have observable impacts on ocean surface roughness, wind stress, air–sea interactions, global climate, and possibly mixing in the global ocean [3–7]. As a result, research on swells recently became a subject of increasing interest in the discipline of ocean science [8,9]. However, there is still little quantitative research on this topic, and the processes that control swell evolution on large scales remain unclear.

Based on the coherent persistence of swells along their propagation routes, synthetic aperture radar (SAR) was shown to be an effective approach to track swells across the ocean [10–12]. Jiang et al. [13] successfully tracked the propagation of storm swells from source regions around 58°S, 132°W to the coast of Mexico using SAR wave mode data. Ardhuin et al. [2] observed the

dissipation of swell energy from a number of storms using high-quality global SAR data, and found that swells propagated distances of 2800 to >20,000 km, depending on the swell steepness. However, SAR sampling cannot be applied when mismatched to the natural swell propagation. Consequently, Ardhuin et al. obtained only 22 total estimates of the swell energy budget at peak periods of 13–18 s from 10 storms recorded during the period 2003–2007.

Because typhoon-induced swells seldom propagate across any measurement array that is deployed in advance, it can be difficult to observe them using in situ measurements. To date, to our knowledge, only the experiment of Snodgrass et al. [1] and the measurements of wind-wave growth and swell decay during the Joint North Sea Wave Project (JONSWAP) by Hasselmann et al. [14] were able to investigate swell evolution at large scales. Therefore, observational studies of swell propagation are relatively scarce.

In recent years, a new method of observing swells emerged, based on seismic records of typhoon-generated noise (i.e., “microseisms”) [15–20]. Seismic noise is used here as a proxy for swell monitoring in areas where ocean wave gauges are poorly instrumented. This interdisciplinary approach, spanning ocean acoustics, marine geophysics, and physical oceanography, could also remotely sense the propagation of swells generated by typhoons, with a focus on locating the source area and estimating the origin times of swells. This is expected to complement existing observational methods and numerical simulations of swells.

Microseisms are the most energetic component of seismic noise, with a typical frequency peak of ~0.05–0.4 Hz [21–23]. Ocean wave activity was long accepted as the major source of microseisms [24]. A portion of the energy inherited from ocean waves at the sea surface (e.g., generated by typhoons) can propagate to the sea floor or shoreline and be transferred to seismic waves in basement rocks as microseisms. These microseisms can propagate as both surface waves (mainly Rayleigh) and compressional (*P*) waves, which can be recorded by broadband seismometers located thousands of kilometers from the source [25–28]. Recent studies also reported Love waves and *S* waves detected in microseismic signals [29,30].

Microseisms can be divided into two distinct bands in the frequency domain, which are called single-frequency (SF, ~0.05–0.12 Hz) and double-frequency (DF, ~0.12–0.4 Hz) microseisms. Each band is generated by a different physical process. SF microseisms are generated by the direct interaction of pressure fluctuations induced by ocean waves with the shallow seafloor or the shore, and therefore, typically have energy concentrated in the same frequency band as ocean waves [31]. Because ocean-wave-induced pressure fluctuations attenuate exponentially with water depth with an e-folding constant equal to the wavenumber [32], the source regions of SF microseisms are generally areas of shallow coastal water. DF microseisms are observed at higher intensities than SF microseisms and are characterized by dominant frequencies of approximately twice the corresponding ocean wave frequencies. They are generated by depth-independent seafloor pressure fluctuations that are induced by the nonlinear interference of ocean waves with nearly opposite propagation directions at similar periods [24]. Based on the Longuet-Higgins theory, Ardhuin et al. [33] developed the first numerical model of DF microseism generation by random ocean waves and presented a classification system for DF microseism generation from wave–wave interactions under typhoon conditions. In their classification, Class-I microseisms are produced by interactions between opposing ocean waves generated by a rapidly moving typhoon at different times, Class-II microseisms are caused by the interaction between typhoon-induced swells incident on coasts and their coastal reflections, and Class-III microseisms arise from interactions between ocean waves generated by two distinct typhoons.

DF microseisms could be used to monitor typhoons and to track typhoon-induced swells [25,28,34–36], because typhoon-induced swells are dispersive surface gravity waves that propagate in deep water over long distances. The swells can reach and impact coastlines, generating dispersive DF microseisms due to interactions between incident swells and opposing components from coastal reflection. Consequently, the time–frequency evolution of dispersive DF microseisms is closely related to the dispersion of typhoon-induced swells, and can, therefore, provide a potential

way to characterize the propagation of typhoon-induced swells, which are rarely observed using conventional equipment.

To our knowledge, Barruol et al. [17,18], Cathles et al. [19], and Davy et al. [20] are the only existing studies that used seismic signals to remotely detect typhoon-induced ocean swells. Specifically, Barruol et al. [17,18] used seismic stations as alternatives to ocean wave buoys for analyzing ocean wave activity, employing microseisms to estimate swell height and propagation direction through polarization analysis. Cathles et al. [19] used seismic observations of 93 distant ocean swell events recorded on the Ross Ice Shelf during 2004–2006 to demonstrate that typhoon-induced swells could have a tangible mechanical influence on the calving margins of the Antarctic Ice Sheet. Davy et al. [20] investigated microseisms of extreme swell events recorded on La Réunion island using seismic stations as ocean wave gauges, verifying that microseisms can provide valuable insights into extreme swell events. Although both Barruol et al. [17,18] and Davy et al. [20] proposed retrieving the swell propagation direction from the azimuth of the seismic noise using polarization analysis, these studies treated the origin of each swell as a static point, rather than a dynamic feature with a distributed source whose centroid changes with the temporal evolution of a typhoon.

Approximately 30% of tropical cyclones occur in the northwest Pacific, which makes this an ideal study area [37,38]. Typhoon Megi was one of the most intense typhoons in the northwest Pacific during 2010, with Category 5 strength on the Saffir–Simpson hurricane wind scale. The present work is a proof-of-concept study for investigations of typhoon-induced ocean swell origins during the lifespan of Typhoon Megi, using seismic data recorded in coastal areas. We first investigated the DF microseisms recorded during Typhoon Megi by terrestrial seismic stations on Taiwan and the Ryukyu Islands. We then inverted for the origin time and source region of typhoon-induced swells using the dispersion characteristics of DF microseisms, and obtained results that are generally consistent with ERA5 reanalysis of ocean wave data. This demonstrates that seismic monitoring could allow us to track typhoon-induced swells using microseisms recorded at coastal sites.

2. Data

According to the best-track data of the Regional Specialized Meteorological Center (RSMC), Megi formed over the deep Philippine Sea on 13 October 2010, and intensified to super typhoon classification, with 10-min maximum sustained wind speeds up to ~230 km/h recorded early on 18 October 2010. Megi moved into the South China Sea (SCS), then turned north to the Taiwan Strait after making landfall on Luzon Island, Philippines on 18 October 2010, and made a second and final landfall in southeast (SE) China on 23 October (Figure 1). The long track course of Megi, with a principally westward-moving direction over the deep Philippine Sea, provided ample opportunity to generate intense ocean swells propagating toward Taiwan and the Ryukyu Islands. The subsequent DF microseisms were used here to track typhoon-induced swells using seismological methods.

Continuous vertical-component seismic waveform data recorded by stations in Taiwan and the Ryukyu Islands were obtained from the Incorporated Research Institutions for Seismology (IRIS) Data Management Center and the F-net network of Japan (Figure 1). The ERA5-reanalyzed ocean wave data used in this paper were provided by the ECMWF. Downloaded data covered the period of 10–23 October 2010, comprising the lifespan of Typhoon Megi and three days prior to its onset.

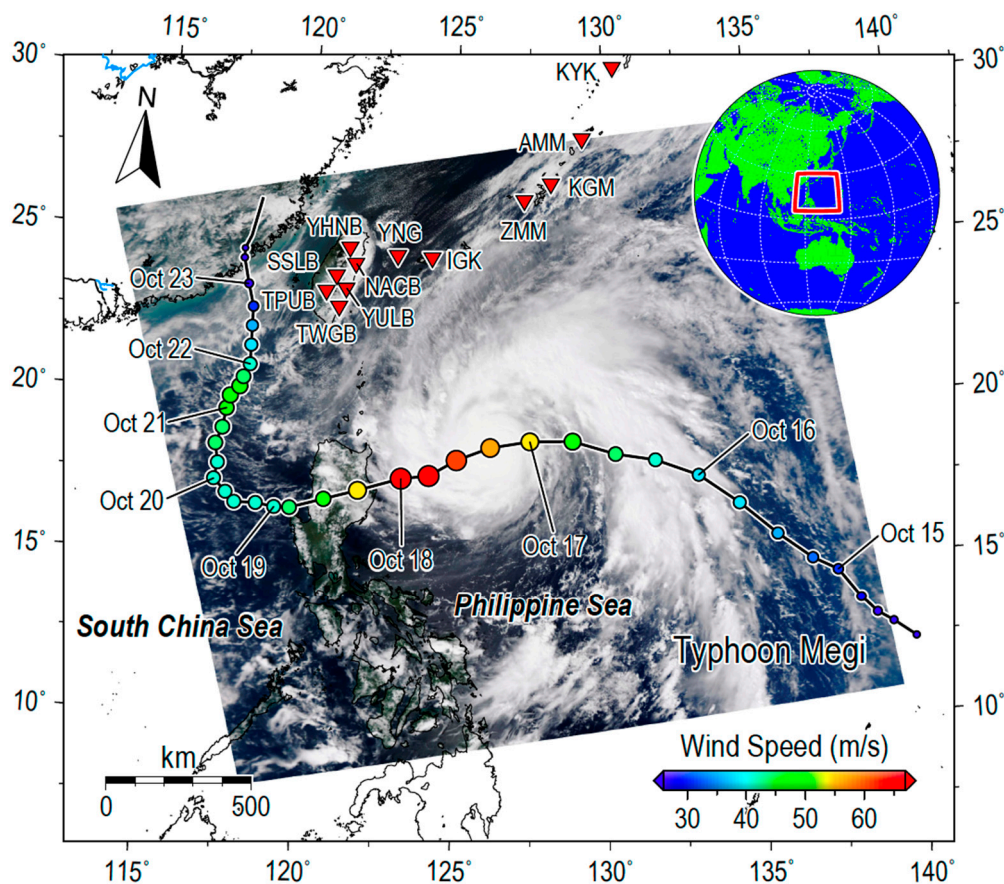


Figure 1. Distribution of seismic stations (red triangles) and trajectory of Typhoon Megi (colored circles) in the western Pacific Ocean, with a superimposed Quick-Look image of Megi captured by Modis on 17 October 2010 at 04:55 coordinated universal time (UTC) (<https://ladsweb.modaps.eosdis.nasa.gov>). The seismic stations are mostly from the Broadband Array in Taiwan for Seismology (BATS) and the F-net network of Japan. The typhoon track is indicated by rounded circles, equally spaced in time at six-hour intervals, with circle size and color related to wind speed. The best-track data of Megi were provided by the Japan Meteorological Agency (<http://www.jma.go.jp/jma/jma-eng/jma-center/rsmc-hp-pub-eg/trackarchives.html>).

To investigate the characteristics of the microseisms generated by typhoon-induced swells, power spectrograms were computed from seismic data to reveal the intensity of the microseisms as a function of time and frequency. Firstly, the original seismic waveform data were preprocessed with the following steps: (1) demeaning and detrending; (2) removal of the instrument response; (3) resampling to one point per second; and (4) filtering with a band-pass filter from 0.05 to 0.45 Hz. Secondly, spectrograms were calculated from preprocessed data using a Fourier transform with a moving-window length of 2048 samples shifted in steps of 1800 samples (i.e., half an hour). Figure 2 shows sample power spectrograms recorded during Typhoon Megi at the seismic stations indicated by red triangles in Figure 1. The spectrograms effectively detected the DF microseisms generated by Megi, and were uncontaminated by transient events such as earthquakes, instrumental irregularities, and non-stationary noise, which appear as short pulses later in the spectrograms. The plots show the temporal evolution of recorded microseisms during the course of Megi. The dispersive DF microseismic signals inspired the investigation of the generation and propagation of typhoon-induced swells using seismological observations.

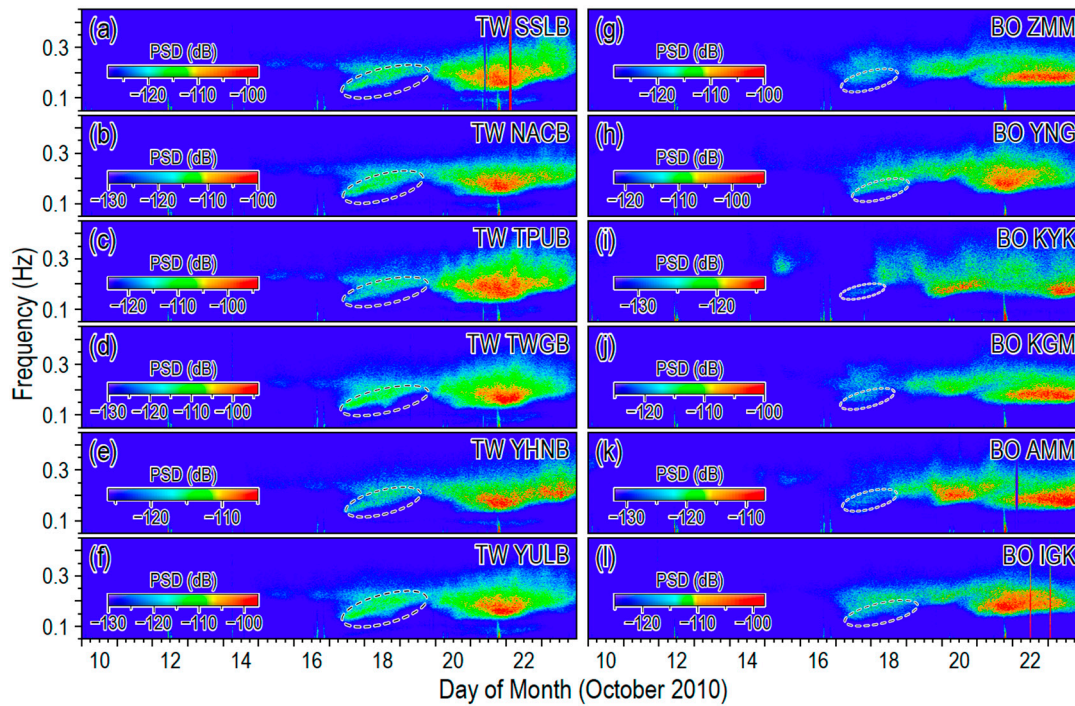


Figure 2. Spectrograms of microseisms from Typhoon Megi recorded by seismic stations (vertical component) on (a–f) Taiwan and (g–l) the Ryukyu Islands. The dashed ellipses outline Class-II (dispersive double-frequency (DF)) microseisms generated in coastal regions. Color scales vary from plot to plot to emphasize the dispersive characteristics of the DF microseisms at each station. The scaling unit (dB) corresponds to $10 \cdot \log_{10}(\text{m}^2/\text{Hz})$.

3. Methods

Our overarching goal was to remotely sense the generation of typhoon-induced swells via dispersive DF microseisms. To that end, we firstly detected the arrivals of typhoon-induced swells using the principal function of the spectrograms calculated before analysis. We then identified the DF (Class-II) microseisms using the swaths of relatively high signal energy density that tilt from lower-left to upper-right (indicating dispersion) in Figure 2 (dashed ellipses).

3.1. Location and Timing of Swell Origin

We calculated great-circle distances and travel times of typhoon-induced swell propagation from the origin to the coastlines, where coastal seismic stations are deployed in the vicinity, based on the method presented by Munk et al. [39].

Typhoon-induced swells propagating on deep water could be considered as surface gravity waves. According to the linear theory for waves forced by gravity, the group velocity could be expressed by

$$C_g = \frac{1}{2} \sqrt{\frac{g\lambda}{2\pi}} = \frac{g}{4\pi} T, \quad (1)$$

where $g = 9.81 \text{ m} \cdot \text{s}^{-2}$ is acceleration due to gravity, λ is wavelength, and T is wave period. Therefore, the group velocity increases with the period in deep water. Assuming ocean swells with frequency f_w propagate a distance x , the corresponding travel time t could be computed as follows:

$$t = \frac{x}{C_g} = \frac{4\pi x}{g} f_w. \quad (2)$$

The partial derivative from Equation (2) is

$$\frac{dt}{df_w} = \frac{4\pi x}{g}. \quad (3)$$

Thus, the ocean swell propagation distance could be derived by

$$x = \frac{g}{4\pi} \left(\frac{df_w}{dt} \right)^{-1}. \quad (4)$$

Because the frequencies of DF microseisms are nearly twice those of the corresponding ocean swells [24], when the ocean swell frequency f_w in Equation (4) is replaced with the DF microseism frequency, the swell propagation distance will be

$$x = \frac{g}{2\pi} \left[\frac{df}{dt} \right]^{-1}, \quad (5)$$

where f is the frequency of the recorded dispersive DF microseisms in Hz; df/dt represents the time–frequency slope that can be calculated using the fractional Fourier transform (FrFT; see Section 3.2) based on the calculated spectrograms.

Similarly, according to Equation (2), the corresponding travel time of the swells could also be expressed with the DF microseism frequency as follows:

$$t = \frac{2\pi f}{g} x. \quad (6)$$

Therefore, we firstly computed the slope of the characteristic frequency of the dispersive DF microseisms versus time df/dt on the basis of the calculated power spectrograms. Then, we could determine the propagation distance x of the swells according to Equation (5), and estimate the travel time using Equation (6).

Figure 3 shows a diagram of the generation of dispersive Class-II DF microseisms by typhoon-induced swells, which are frequency-dispersed after long-distance propagation, and summarizes the geometry of the dispersive DF microseisms depicted in the spectrograms. To calculate swell propagation distance x and travel time t , the linear swath of high signal intensity in the spectrogram is identified by visual inspection and defined as indicated by the rhomboidal shape in Figure 3b. In our preliminary study of the characteristics of microseisms generated by Typhoon Megi [28], dispersive DF microseisms generated in coastal source regions were distributed mainly below 0.2 Hz. Therefore, the upper frequency limit of the inspected region was set to 0.18 Hz here, which could be regarded as the boundary between the dispersive (pink ellipse in Figure 3b) and non-dispersive (blue-gray ellipse) microseisms.

We emphasized the dispersive characteristics using three additional processing steps. (1) A least-squares regression was used to fit a line to the dominant energy of the inspected region (red line in Figure 3b); i.e., the point (t, f) with the highest spectral amplitude $S(t, f)$ at each time t in the selected region. (2) Points (t, f) distributed below the regression line were selected for further processing and were defined as the FrFT region in Figure 3b. (3) Finally, we applied an FrFT to process the dispersive DF microseisms, to compute df/dt in Equation (5), and thereby, to determine x . Since the swell origin is a complicated air–sea interaction process, which spreads over significant distances and time as the typhoon moves and evolves, the time length of the moving window for the FrFT calculation was set to three hours, during which we assumed that the swell origin was quasi-constant in time and space.

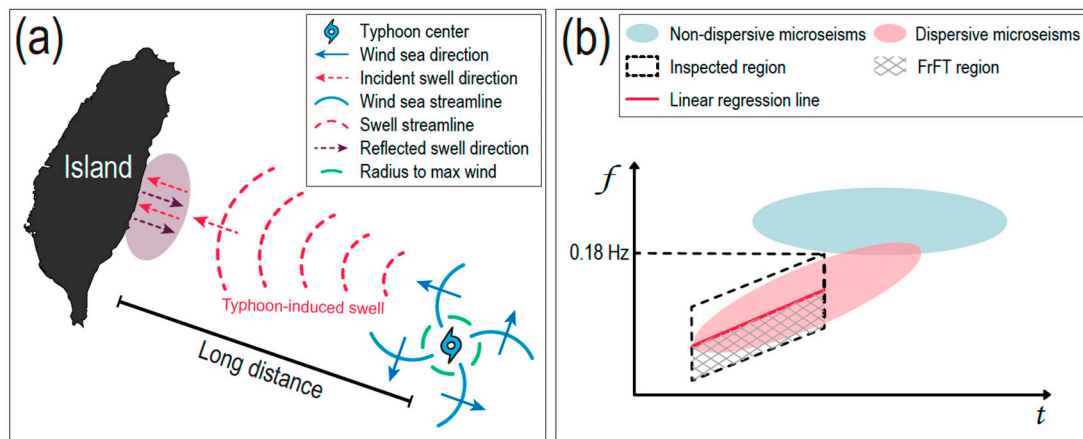


Figure 3. Schematic of (a) DF microseism generation by typhoon-induced swells, and (b) dispersive DF microseisms as they would appear on a spectrogram. When the typhoon-induced swells propagate through deep water over long distances, high-frequency components travel more slowly than low-frequency components, and consequently, the observed DF microseisms are frequency-dispersed, with an energy distribution (pink ellipse) tilting from lower-left to upper-right. For interpretation, see the text.

3.2. Fractional Fourier Transform

The fractional Fourier transform (FrFT) was introduced by Namias [40] and is now widely applied in various fields of study as a rotation operator in the time–frequency plane [41,42]. The FrFT is suitable for analyzing linear frequency-modulated (LFM) signals due to their energy concentration, as they have linear instantaneous frequencies in a subregion of their total bandwidth. The FrFT is defined by the transformation kernel $K_\alpha(t, u)$; for an LFM signal $x(t)$, this can be expressed by

$$X_\alpha(u) = \int_{-\infty}^{\infty} x(t)K_\alpha(t, u)dt, \quad (7)$$

$$K_\alpha(t, u) = \begin{cases} \sqrt{1 - i \cot \alpha} \exp(i2\pi(\frac{t^2+u^2}{2} \cot \alpha - \frac{tu}{\sin \alpha})) & \alpha \neq n\pi \\ \delta(t - u) & \alpha = 2n\pi \\ \delta(t + u) & \alpha = (2n + 1)\pi \end{cases}, \quad (8)$$

where α is the angle used to apply a rotational transformation to the conventional time–frequency axes. The optimal α value yields the highest-magnitude response to the LFM signal. According to Reference [43], the optimal transform angle α is numerically related to the rate of the LFM signal χ by

$$\alpha = -\arctan\left(\frac{F_s^2/\Omega}{2\chi}\right), \quad (9)$$

where F_s is the sampling rate and Ω is the total number of time samples. The frequency-versus-time slope in this paper, df/dt , was computed from χ according to Equation (9).

4. Results and Discussion

4.1. Swell-Generated DF Microseisms

The DF microseisms generated by Typhoon Megi were detected effectively on spectrograms (Figure 2), with little contamination. Occasional high-amplitude transient events, such as earthquakes, instrumental irregularities, and non-stationary noise, appeared as short pulses on the spectrograms. Before 17 October 2010, when the typhoon center was still over the deep Philippine Sea (Figure 1), we

observed weak DF microseisms above 0.2 Hz, which were shown to have Class-I source mechanisms and centroids around the typhoon center [28].

Figure 4 shows the distributions of the peak periods of ocean waves when Typhoon Megi was still over the Philippine Sea. The majority of typhoon-induced swells propagated nearly westward, to Taiwan and Luzon islands. Because of the dispersive effects of surface gravity waves on deep water, the low-frequency waves (deep red color in Figure 4) propagated at a higher group velocity than the high-frequency components, thus arrived and interacted earlier with the coasts to generate low-frequency DF microseisms.

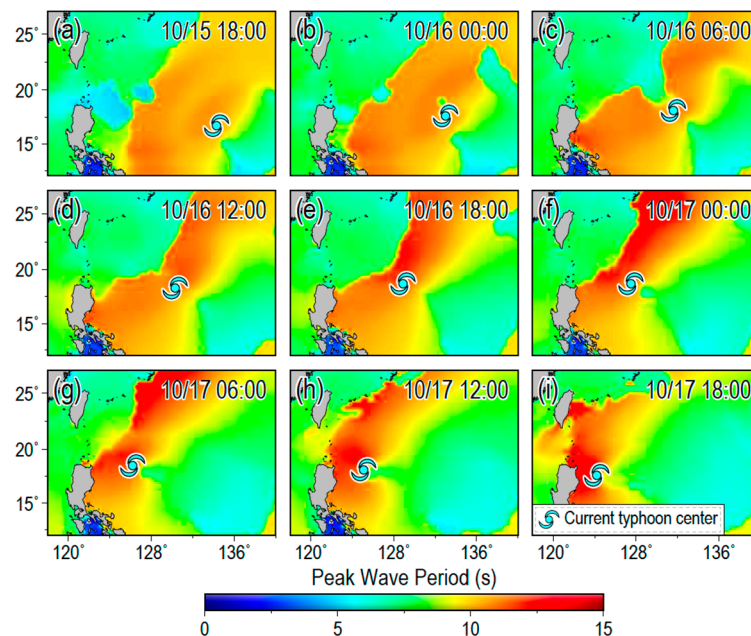


Figure 4. Analysis of the propagation and dispersion of ocean swells induced by Typhoon Megi. The distribution of peak periods of ocean waves in 6-h time intervals on 15–17 October 2010 (a–i) was predicted by ERA5 reanalysis from the European Centre for Medium-Range Weather Forecasts (ECMWF), and hurricane symbols indicate the location of the typhoon center at each time.

DF microseisms were observed on 17–18 October 2010 with dominant frequencies that increased almost linearly from 0.12 to 0.20 Hz (Figure 2). In our preliminary study [28], we noted that these DF microseisms were expected to originate near local coasts (i.e., along the SE coast of Taiwan) due to interactions between reflected ocean swells and subsequent incident swells. This is consistent with the propagation of typhoon-induced swells shown in Figure 4. The onset of these dispersive DF microseisms in the late afternoon of 17 October 2010 was in good agreement with the time when the first low-frequency swells arrived at the eastern coastline of Taiwan. The time–frequency characteristics of these DF microseisms reflect the dispersion of the corresponding ocean swells, and could, thus, be used as a proxy to explore the generation and propagation of typhoon-induced swells.

4.2. Origins of Typhoon-Induced Swell

The derived propagation distances of the typhoon-induced swells were compared with the distances from the seismic stations to the typhoon centers indicated by the best-track data (Figure 5). The correlation coefficients (CC) between the least-squares regression lines (pink lines in Figure 5a–f) and the corresponding dominant energy points (i.e., the points (t, f) with the highest spectral amplitude $S(t, f)$ at each time t) in the inspected region were all above 0.8, indicating linear dispersion of the DF microseisms. However, when the slope of the least-squares regression line was used in Equation (5) directly, we found that the estimated swell source regions were located at a distance (~1000 km) from the trajectory of Megi (Figure 5g–l). It is likely that the typhoon moved significantly

over this long time interval, and the induced ocean waves, thus, developed into ocean swells at locations far from the typhoon trajectory. Therefore, the inspected region was segmented into three-hour time windows, during which the typhoon was assumed to move minimally and the swell origin was constrained to a quasi-static region in space and time. The FrFT was then computed for each successive segment of DF microseisms to obtain the corresponding swell propagation distance. We find that these distances are generally coincident with the locations of the typhoon center after 15 October 2010, when Megi strengthened to become a typhoon (Figure 5g–l).

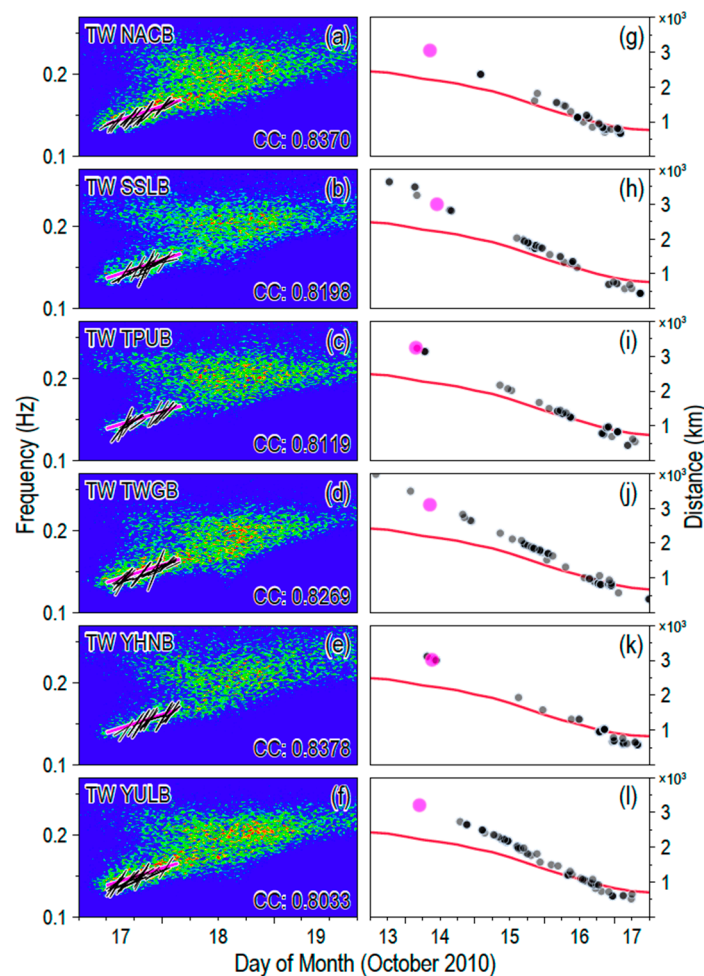


Figure 5. Estimation of the propagation distance x of typhoon-induced swells from the origin to the Taiwan coastline based on seismic records. (a–f) Dispersive DF microseisms generated by the ocean swells induced by Typhoon Megi on power spectrograms computed using data from seismic stations in Taiwan. The pink solid lines superimposed on the spectrograms represent least-squares regression lines as in Figure 3b, and dark lines denote the calculated slope df/dt of the dispersive DF microseisms in successive three-hour time windows. (g–l) Comparison between estimated propagation distances of typhoon-induced swells and distances from the typhoon center to seismic stations (red lines). Large pink dots and small gray dots represent calculated propagation distances using the pink and dark lines in the subfigures in the left column, respectively.

Figure 6 shows the propagation distance x , the initial wave period T , and the origin time t_2 of the typhoon-induced swells derived from the dispersion characteristics of DF microseisms recorded by station YULB, which is located close to the coastline (~ 18 km) of eastern Taiwan (Figure 1). Probable source regions are indicated by dotted circles with their centers at the station location and their radii equal to the propagation distance x . We assumed that the most likely source regions of long-period ocean swells had the highest-amplitude significant wave heights, and therefore, we superimposed

the significant height of the total swell predicted by ERA5 reanalysis at time t_1 , which was close to the calculated swell origin time t_2 , in Figure 6a–c. Furthermore, the corresponding peak wave period, which reports the wave fronts of the long-period ocean swells, was superimposed on the plots of Figure 6d–f. We compared the origins of typhoon-induced swells calculated from DF microseisms with ocean-wave state data provided by ERA5 reanalysis and found good consistency between the two estimates. These results indicate that the dispersion characteristics of DF microseisms recorded by coastal seismic stations could be a useful proxy for tracking and monitoring typhoon-induced swells over oceans.

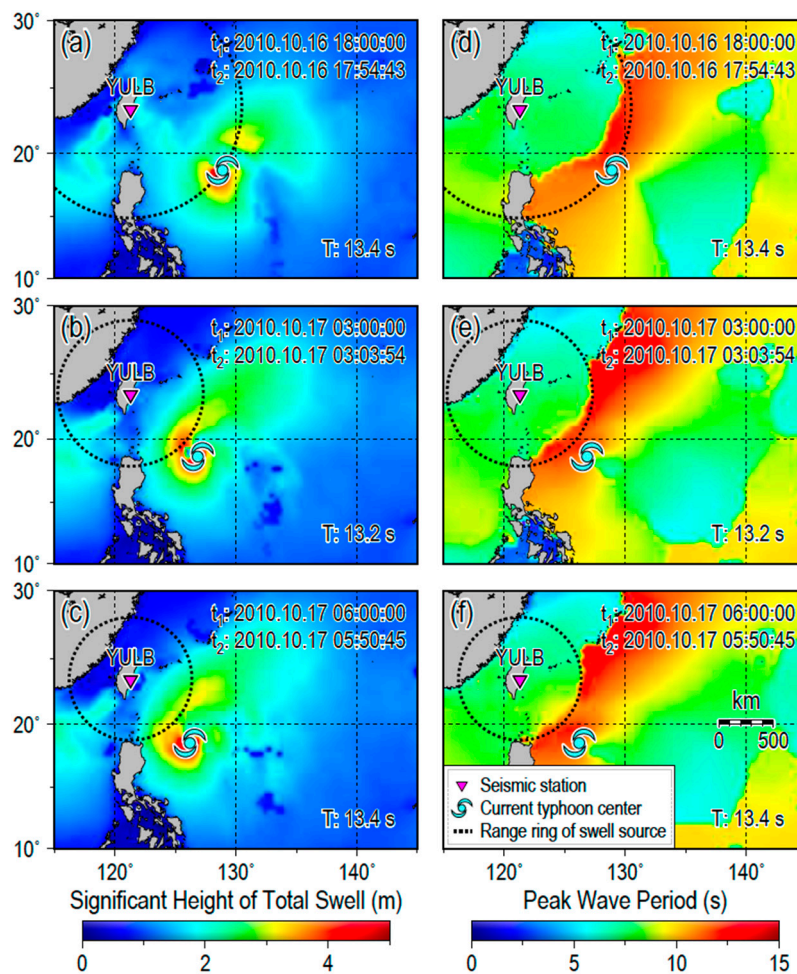


Figure 6. Typhoon-induced swell propagation calculated from dispersive DF microseisms at station YULB, compared with (a–c) significant heights of total swells and (d–f) peak wave periods at time t_1 as predicted by ERA5 reanalysis. The dotted circle centered on station YULB, with radius equal to the propagation distance x , represents the probable location of the origin of each swell. The origin time and initial wave period of the typhoon-induced swell are denoted t_2 and T , respectively, and the hurricane symbols indicate the locations of the typhoon center.

4.3. Localization Deviations

The effective generation of dispersive DF microseisms depends on the properties of the coastlines, where reflected and incident typhoon-induced swells interact to generate DF microseisms. For example, the DF microseisms that we observed were weaker in the Ryukyu Islands than in Taiwan, as shown in Figure 2. It is likely that the coastlines of the Ryukyu Islands are not long enough to produce the strong reflections necessary for strong DF microseisms. Consequently, coastal seismic stations in eastern Taiwan, such as station YULB, were primarily used in this study. In addition, the geometry of the

coastlines has a strong influence on the generation of DF microseisms [44], as such microseisms can only be generated effectively when incident ocean swells are reflected in the opposite direction by the coast, and subsequently, interfere with later incident swells. Figure 7 shows several coastline geometries that could contribute effectively to the generation of DF microseisms. The topographic properties of the coastlines, such as steepness, will also affect the reflection coefficients of incident swells and further affect the efficiency of the generation of DF microseisms, as described by Ardhuin et al. [33]. In addition, the effective generation of dispersive DF microseisms depends on the intensity of the incident ocean swells; e.g., before Megi strengthened into a typhoon, its induced ocean waves and swells were not strong enough to generate DF microseisms at high signal-to-noise ratios (SNRs) in Taiwan. Consequently, the computed swell propagation distances were not so consistent with the locations of the typhoon center for the period before 15 October 2010 (Figure 5).

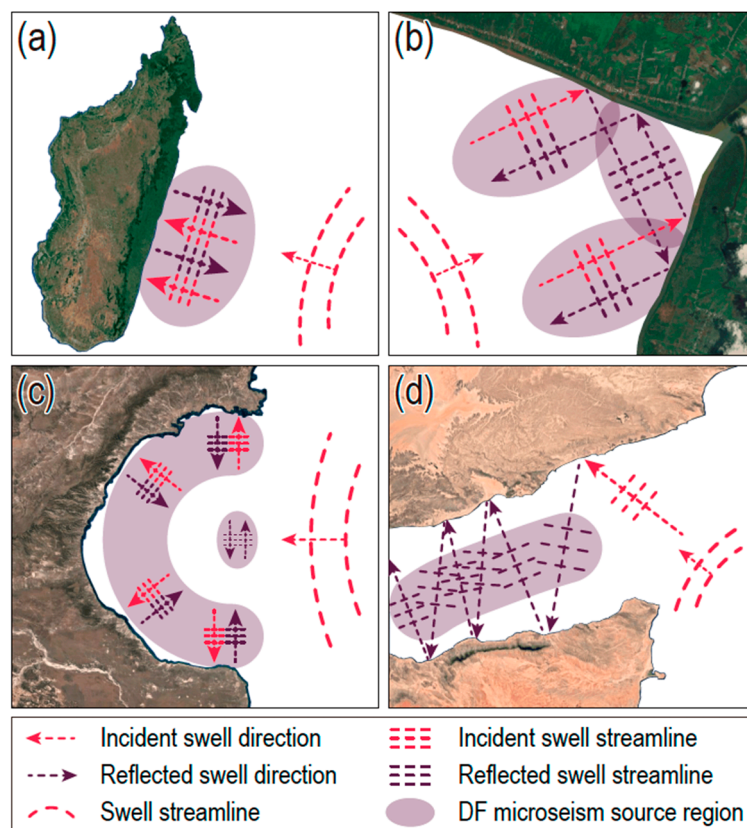


Figure 7. Examples of coastline geometries that facilitate the generation of dispersive DF microseisms, including (a) straight coast, (b) rectangular coast, (c) bay, and (d) channel. In all cases, the coast provides opportunities for interference between incident and reflected ocean waves with similar periods. Landscape images were downloaded from Google Maps.

Furthermore, the geographic locations of seismic stations have considerable influence on the effectiveness of our method for tracking typhoon-induced swells. Figure 8 shows a possible source of error in our localization method caused by the location of a seismic station relative to the coast. The calculated propagation distance x of the typhoon-induced swell is theoretically expected to equal the true propagation distance r from the swell source region to the coastal source of the DF microseisms. However, in the localization process, the derived source regions of ocean swells are restricted to an arc of radius x centered on the seismic station rather than the coast. Hence, the distance vector from the seismic station to the source of the DF microseisms contributes to the localization misfit. Further investigation of the coastal source regions of the dispersive DF microseisms is necessary to evaluate and correct these deviations, and such an effort is essential to improve this method.

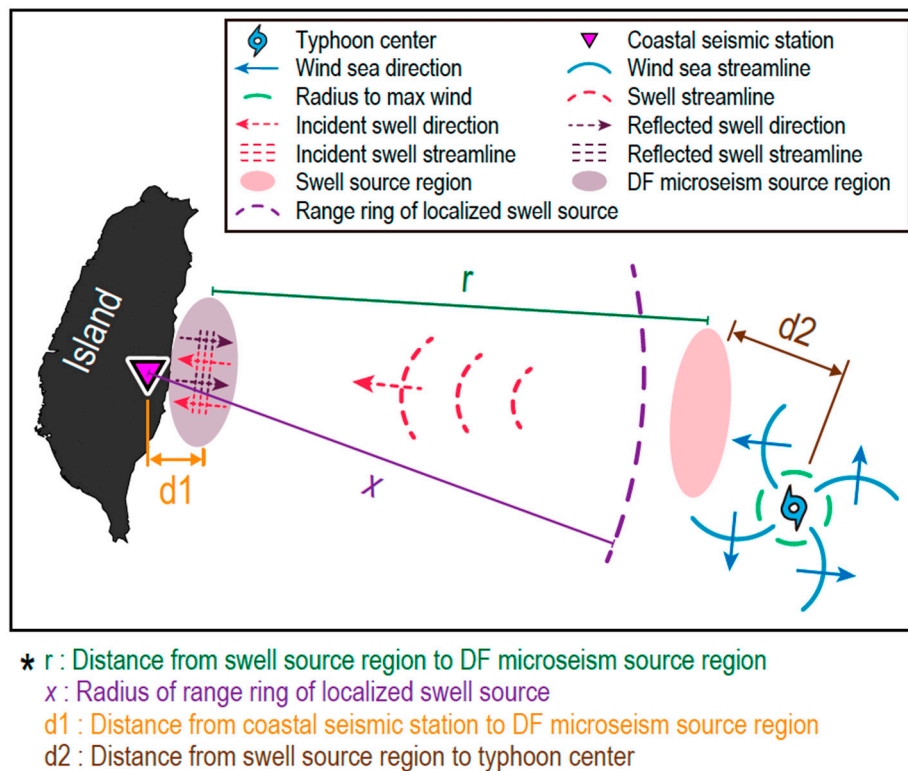


Figure 8. Schematic diagram of the analysis of the ocean swell localization deviation due to the geographic location of the seismic station.

From our preliminary investigation [28], DF microseisms with coastal sources propagate inland and gradually attenuate; thus, coastal stations generally record stronger DF microseisms than inland sites. Therefore, the distance inland of the seismic station plays an important role in determining the SNR. For example, stations located relatively close to the eastern coast of Taiwan, such as YULB, NACB, and TWGB, detected stronger dispersive DF microseisms (Figures 2 and 5). This is one of the principal reasons why station YULB was used in this study. In addition, the detection and calculation of dispersive DF microseisms are affected by local background noise, including undesirable signals induced by local site effects.

Finally, localization deviations could also be affected by the accuracy of the fundamental assumptions of this method. The ocean swell propagation distance x is calculated from the frequency dispersion relationship of the ocean swells, and is directly used in computing the great-circle distance from the observation site to the swell source region. However, the actual propagation route of the swells can be affected by factors including sea surface winds, ocean currents, wave–wave interactions, and seafloor topography near the coast, leading to deviations of the propagation path from an idealized great circle. As a result, as typhoon-induced swells propagate farther, and these factors increasingly affect the deviation, resulting in larger errors in the localization of swell source regions, as shown in Figure 5.

5. Conclusions

Ocean swells induced in the western Pacific Ocean by Typhoon Megi in 2010 were tracked effectively using DF microseisms recorded by seismic stations in eastern Taiwan. The frequency dispersion of the DF microseisms was used to calculate the propagation distance and constrain the source regions of ocean swells. Localized source regions and calculated wave periods of ocean swells were generally consistent with ocean-wave field data provided by ERA5 reanalysis from ECMWF. Although localization results can depend on the effective detection of dispersive DF microseisms, which is tied to both coastline geometry and the locations of the seismometers, the present results

indicate that the dispersion characteristics of DF microseisms recorded by coastal seismometers could be a viable proxy measure for tracking and monitoring typhoon-induced swells across the oceans.

Author Contributions: Conceptualization, J.L., X.L., and H.Z. Data curation, S.F. Formal analysis, J.L., S.F., and H.Z. Investigation, S.F. Methodology, J.L. and H.Z. Project administration, J.L. Supervision, J.L. and X.L. Visualization, S.F. and R.W. Writing—original draft, J.L. Writing—review and editing, J.L., X.L., and H.Z.

Acknowledgments: Seismic waveform data used in this study are freely available from the IRIS Data Management System (www.iris.edu) and the F-net network of Japan (www.fnet.bosai.go.jp). MODIS data are provided by NASA (National Aeronautics and Space Administration, USA). ERA5 reanalysis of ocean wave data from ECMWF was accessed at <http://apps.ecmwf.int/data-catalogues/era5>. The best-track data of the RSMC were accessed at http://www.jma.go.jp/jma/jma-eng/jma-center/rsmc-hp-pub-eg/RSMC_HP.htm. Some of the figures were generated using the Generic Mapping Tools (GMT) software [45]. The manuscript benefited from thoughtful discussions with Hanhao Zhu. This work was supported by the Natural Science Foundation of Zhejiang Province (LZ14D060001). The views, opinions, and findings contained in this report are those of the authors and should not be construed as an official NOAA or US Government position, policy, or decision.

Conflicts of Interest: The authors declare no conflicts of interest.

References

1. Snodgrass, F.E.; Groves, G.W.; Hasselmann, K.; Miller, G.R.; Munk, W.H.; Powers, W.H. Propagation of ocean swell across the Pacific. *Philos. Trans. R. Soc. Lond. Ser. A* **1966**, *249*, 431–497. [[CrossRef](#)]
2. Ardhuin, F.; Chapron, B.; Collard, F. Observation of swell dissipation across oceans. *Geophys. Res. Lett.* **2009**, *36*. [[CrossRef](#)]
3. Grachev, A.A.; Fairall, C.W. Upward momentum transfer in the marine boundary layer. *J. Phys. Oceanogr.* **2001**, *31*, 1698–1711. [[CrossRef](#)]
4. Babanin, A.V. On a wave-induced turbulence and a wave-mixed upper ocean layer. *Geophys. Res. Lett.* **2006**, *33*. [[CrossRef](#)]
5. Hwang, P.A. Observations of swell influence on ocean surface roughness. *J. Geophys. Res.* **2008**, *113*. [[CrossRef](#)]
6. Semedo, A. Atmosphere-Ocean Interactions in Swell Dominated Wave Fields. Available online: <http://www.diva-portal.org/smash/record.jsf?pid=diva2%3A350126&dswid=4604> (accessed on 6 September 2018).
7. Wu, L.; Rutgersson, A.; Sahlee, E.; Guo Larsen, X. Swell impact on wind stress and atmospheric mixing in a regional coupled atmosphere-wave model. *J. Geophys. Res. Oceans* **2016**, *121*, 4633–4648. [[CrossRef](#)]
8. Smedman, A.S.; Höglström, U.; Sahlé, E.; Drennan, W.M.; Kahma, K.K.; Pettersson, H.; Zhang, F. Observational study of marine atmospheric boundary layer characteristics during swell. *J. Atmos. Sci.* **2009**, *66*, 2747–2763. [[CrossRef](#)]
9. Höglström, U.; Smedman, A.S.; Semedo, A.; Rutgersson, A. Comments on “A global climatology of wind-wave interaction”. *J. Phys. Oceanogr.* **2011**, *41*, 1811–1813. [[CrossRef](#)]
10. Li, X.; Zhang, J.A.; Yang, X.; Pichel, W.G.; DeMaria, M.; Long, D.; Li, Z. Tropical cyclone morphology from spaceborne synthetic aperture radar. *Bull. Am. Meteorol. Soc.* **2012**, *94*, 215–230. [[CrossRef](#)]
11. Li, X. The first Sentinel-1 SAR image of a typhoon. *Acta Oceanol. Sin.* **2015**, *34*. [[CrossRef](#)]
12. Li, X.; Pichel, W.G.; He, M.; Wu, S.; Friedman, K.S.; Clemente-Colon, P.; Zhao, C. Observation of hurricane-generated ocean swell refraction at the Gulf Stream north wall with the RADARSAT-1 synthetic aperture radar. *IEEE Trans. Geosci. Remote Sens.* **2002**, *40*, 2131–2142.
13. Jiang, H.; Stopa, J.E.; Wang, H.; Husson, R.; Mouche, A.; Chapron, B.; Chen, G. Tracking the attenuation and nonbreaking dissipation of swells using altimeters. *J. Geophys. Res. Oceans* **2016**, *121*, 1446–1458. [[CrossRef](#)]
14. Hasselmann, K.; Barnett, T.P.; Bouws, E.; Carlson, H.; Gartwright, D.E.; Enke, K.; Ewing, J.A.; Gienapp, H.; Hasselmann, D.E.; Kruseman, P.; et al. Measurements of wind-wave growth and swell decay during the Joint North Sea Wave Project (JONSWAP). *Dtsch. Hydrogr. Z. Suppl.* **1973**, *12*, 1–95.
15. Bromirski, P.D.; Flick, R.E.; Graham, N. Ocean wave height determined from inland seismometer data: Implications for investigating wave climate changes in the NE Pacific. *J. Geophys. Res. Oceans* **1999**, *104*, 20753–20766. [[CrossRef](#)]
16. Okal, E.A.; MacAyeal, D.R. Seismic recording on drifting icebergs: Catching seismic waves, tsunamis and storms from Sumatra and elsewhere. *Seismol. Res. Lett.* **2006**, *77*, 659–671. [[CrossRef](#)]

17. Barruol, G.; Reymond, D.; Fontaine, F.R.; Hyvernaud, O.; Maurer, V.; Maamaatuaiahutapu, K. Characterizing swells in the southern Pacific from seismic and infrasonic noise analyses. *Geophys. J. Int.* **2006**, *164*, 516–542. [[CrossRef](#)]
18. Barruol, G.; Davy, C.; Fontaine, F.R.; Schlindwein, V.; Sigloch, K. Monitoring austral and cyclonic swells in the “Iles Eparses” (Mozambique channel) from microseismic noise. *Acta Oecol.* **2016**, *72*, 120–128. [[CrossRef](#)]
19. Cathles IV, L.M.; Okal, E.A.; MacAyeal, D.R. Seismic observations of sea swell on the floating Ross Ice Shelf, Antarctica. *J. Geophys. Res. Earth Surf.* **2009**, *114*. [[CrossRef](#)]
20. Davy, C.; Barruol, G.; Fontaine, F.R.; Cordier, E. Analyses of extreme swell events on La Réunion Island from microseismic noise. *Geophys. J. Int.* **2016**, *207*, 1767–1782. [[CrossRef](#)]
21. Haubrich, R.A.; McCamy, K. Microseisms: Coastal and pelagic sources. *Rev. Geophys.* **1969**, *7*, 539–571. [[CrossRef](#)]
22. Bromirski, P.D. Vibrations from the “Perfect Storm”. *Geochem. Geophys. Geosyst.* **2001**, *2*. [[CrossRef](#)]
23. Bromirski, P.D.; Duennebie, F.K.; Stephen, R.A. Mid-ocean microseisms. *Geochem. Geophys. Geosyst.* **2005**, *6*. [[CrossRef](#)]
24. Longuet-Higgins, M.S. A theory of the origin of microseisms. *Philos. Trans. R. Soc. Lond. Ser. A Math. Phys. Sci.* **1950**, *243*, 1–35. [[CrossRef](#)]
25. Gerstoft, P.; Fehler, M.C.; Sabra, K.G. When Katrina hit California. *Geophys. Res. Lett.* **2006**, *33*. [[CrossRef](#)]
26. Gerstoft, P.; Shearer, P.M.; Harmon, N.; Zhang, J. Global P, PP, and PKP wave microseisms observed from distant storms. *Geophys. Res. Lett.* **2008**, *35*. [[CrossRef](#)]
27. Zhang, J.; Gerstoft, P.; Bromirski, P.D. Pelagic and coastal sources of P-wave microseisms: Generation under tropical cyclones. *Geophys. Res. Lett.* **2010**, *37*. [[CrossRef](#)]
28. Lin, J.M.; Lin, J.; Xu, M. Microseisms generated by super typhoon Megi in the western Pacific Ocean. *J. Geophys. Res. Oceans* **2017**, *122*, 9518–9529. [[CrossRef](#)]
29. Tanimoto, T.; Lin, C.J.; Hadziioannou, C.; Igel, H.; Vernon, F. Estimate of Rayleigh-to-Love wave ratio in the secondary microseism by a small array at Piñon Flat observatory, California. *Geophys. Res. Lett.* **2016**, *43*. [[CrossRef](#)]
30. Nishida, K.; Takagi, R. Teleseismic S wave microseisms. *Science* **2016**, *353*, 919–921. [[CrossRef](#)] [[PubMed](#)]
31. Hasselmann, K.A. Statistical analysis of the generation of microseisms. *Rev. Geophys.* **1963**, *1*, 177–210. [[CrossRef](#)]
32. Webb, S.C. Broadband seismology and noise under the ocean. *Rev. Geophys.* **1998**, *36*, 105–142. [[CrossRef](#)]
33. Ardhuin, F.; Stutzmann, E.; Schimmel, M.; Mangeney, A. Ocean wave sources of seismic noise. *J. Geophys. Res.* **2011**, *116*. [[CrossRef](#)]
34. Chi, W.C.; Chen, W.J.; Kuo, B.Y.; Dolenc, D. Seismic monitoring of western Pacific typhoons. *Mar. Geophys. Res.* **2010**, *31*, 239–251. [[CrossRef](#)]
35. Sufri, O.; Koper, K.D.; Burlacu, R.; Foy, B.D. Microseisms from Superstorm Sandy. *Earth Planet. Sci. Lett.* **2014**, *402*, 324–336. [[CrossRef](#)]
36. Lin, J.M.; Wang, Y.T.; Wang, W.T.; Li, X.F.; Fang, S.K.; Chen, C.; Zheng, H. Seismic Remote Sensing of Super Typhoon Lupit (2009) with Seismological Array Observation in NE China. *Remote Sens.* **2018**, *10*, 235. [[CrossRef](#)]
37. Gray, W.M. Global view of the origin of tropical disturbances and storms. *Mon. Weather Rev.* **1968**, *96*, 669–700. [[CrossRef](#)]
38. Lu, X.; Yu, H.; Yang, X.; Li, X. Estimating tropical cyclone size in the Northwestern Pacific from geostationary satellite infrared images. *Remote Sens.* **2017**, *9*, 728. [[CrossRef](#)]
39. Munk, W.H.; Miller, G.R.; Snodgrass, F.E.; Barber, N.F. Directional recording of swell from distant storms. *Philos. Trans. R. Soc. Lond. Ser. A* **1963**, *255*, 505–584. [[CrossRef](#)]
40. Namias, V. The fractional order Fourier transform and its application to quantum mechanics. *IMA J. Appl. Math.* **1980**, *25*, 241–265. [[CrossRef](#)]
41. Yu, J.; Zhang, L.; Liu, K.; Liu, D. Separation and localization of multiple distributed wideband chirps using the fractional Fourier transform. *EURASIP J. Wirel. Commun. Netw.* **2015**, *1*, 1–8. [[CrossRef](#)]
42. Wei, D.; Li, Y.M. Generalized sampling expansions with multiple sampling rates for lowpass and bandpass signals in the fractional Fourier transform domain. *IEEE Trans. Signal Process.* **2016**, *64*, 4861–4874. [[CrossRef](#)]
43. Capus, C.; Brown, K. Short-time fractional Fourier methods for the time-frequency representation of chirp signals. *J. Acoust. Soc. Am.* **2003**, *113*, 3253–3263. [[CrossRef](#)] [[PubMed](#)]

44. Friedrich, A.; Kruger, F.; Klinge, K. Ocean generated microseismic noise located with the Gräfenberg array. *J. Seismolog.* **1998**, *2*, 47–64. [[CrossRef](#)]
45. Wessel, P.; Smith, W.H.F. New improved version of Generic Mapping Tools released. *EOS Trans. AGU* **1998**, *79*, 579. [[CrossRef](#)]



© 2018 by the authors. Licensee MDPI, Basel, Switzerland. This article is an open access article distributed under the terms and conditions of the Creative Commons Attribution (CC BY) license (<http://creativecommons.org/licenses/by/4.0/>).